Inorganic mesoporous silicas as vehicles of two novel anthracene-based ruthenium metalloarenes

Sara Rojas, Francisco J. Carmona, Elisa Barea* and Carmen R. Maldonado*

Department of Inorganic Chemistry, University of Granada, Av. Fuentenueva S/N, 18071 Granada, Spain

Corresponding authors: *Elisa Barea (ebaream@ugr.es), Carmen R. Maldonado (crmaldonado@ugr.es)*

Abstract

Two novel anthracene-based half-sandwich organometallic Ru(II) compounds, namely, [Ru(*p*-cymene)(L_1)Cl_2] (**1**) and [Ru(*p*-cymene)(L_2)Cl_2] (**2**) (**L_1**=1-(anthracen-9-yl)-*N*-(pyridin-3-ylmethyl)methanamine; **L_2**=1-(anthracen-9-yl)-*N*-(pyridin-4-ylmethyl)methanamine) have been synthesized and characterized. We demonstrate that the fluorescence properties of these complexes are highly affected by the linking position of the anthracene unit, as only **2** shows fluorescence emission in the blue region. Regarding their biological activity, both ruthenium metallodrugs show interaction with different biological targets such as S-donor aminoacids (cysteine) and proteases (cysteine cathepsin B). Moreover, **1** and **2** show *in vitro* cytotoxicity against HL-60 cancer cell line (IC_{50} = 84.5 and 87.0 µM for **1** and **2**, respectively), with cell death occurring *via* apoptosis. Further studies have shown that diffusion into cells is the main mechanism of metallodrug uptake. Finally, as a proof of concept, these ruthenium complexes have been succesfully encapsulated into MCM-41 and SBA-15 mesoporous silicas using two different incorporation strategies (impregnation and grinding).

Keywords. Ruthenium metallodrug, fluorescence, MCM-41, SBA-15, cathepsin inhibition, drug encapsulation.

1. Introduction

During the last fifty years, platinum drugs have dominated the field of anticancer therapies. Indeed, cisplatin, carboplatin and oxaliplatin are at present the only metal-based anticancer agents in worldwide clinical use [1]. Whilst the chemotherapeutic success of platinum is manifest, it possesses some remarkable drawbacks, such as: severe dose-limiting side effects, non-anti-metastasic activity, and intrinsic or acquired resistance. Thus, a search for more effective and less toxic metal-based antitumor agents is needed. In this context, many efforts are being directed towards the design of non-conventional antitumor agents based on other transition metals, such as ruthenium. In particular, ruthenium complexes offer some advantages compared to conventional platinum drugs. Firstly, ruthenium has a wide range of oxidation states (Ru^{II}, Ru^{III} and Ru^{IV}), which are accessible under physiological conditions [2], and their complexes are less toxic than the platinum analogues due to the ability of ruthenium to mimic iron in binding to certain biological molecules [3]. On the other hand, ruthenium specifically accumulates in cancer cells [4], and is active against metastasis [5,6]. Finally, these non-conventional metallodrugs show different mechanisms of action towards multiple targets (DNA,[7,8] proteins [9–12], etc.), which may potentially increase the effectiveness of the anticancer treatment.

Another key aspect, that should be noted when designing new metallodrugs, is the possibility of functionalizing these molecules with fluorophores (i.e. anthracene, porphyrins, anthraquinone, phenantroline, etc.) [13–16], in order to confer them trackable properties. In particular, in recent years, Ru-fluorescent compounds are finding numerous applications ranging from imaging to therapeutics, or even both [17]. Very recently, two dinuclear Ru(II) polypyridyl complexes containing three and ten methylene chains have shown cytotoxic activity against HeLa cell line. Their trackable properties have demonstrated that these fluorescent complexes are mainly localized within lysosomes [18]. Another interesting example is a 2-nitroimidazole-ruthenium polypyridyl complex, whose luminescence properties strongly depend on the oxygen concentration. This interesting feature has allowed the detection of hypoxic tissues inside the body [19]. Thus, the development of new Ru-fluorescent compounds would allow the integration of both anticancer therapy and tumour imaging into a single drug for theranostic applications.

On the other hand, in recent decades, many research groups are also focused on the development of biocompatible vehicles that can carry a large payload of drugs and achieve a controlled administration of these bioactive molecules directly into the cells in need of treatment. These encapsulation strategies could also improve the solubility and stability of the designed metallodrugs in biological fluids, avoiding their early degradation

before reaching the cellular target. In this sense, inorganic porous materials, such as mesoporous silicas, are promising candidates because their high surface area to volume ratio, ordered networks, functionalizable pore walls, relative stability, biocompatibility and possibility of preparing them as nanoparticles [20–22]. For example, pH-responsive mesoporous silica nanoparticles (MSNs) loaded with the anticancer drug doxorubicin have been prepared. In fact, in order to achieve a controlled release of this pharmatheutical, acid-decomposable ZnO quantum dots were used to cap the doxorubicin@MSNs [23]. Regarding ruthenium complexes cargo, a recent research describes the development of MSNs with light-triggered delivery of a biologically active ruthenium(II) complex [24,25], while Chen *et al.* have described the synthesis of cancer-targeted monodispersed MSNs as carriers of a Ru-polypyridyl complex. In this work, the strong autofluorescence of the Ru complex has allowed the direct monitoring of drug delivery, and to extend the power of theranostics to subcellular level [26]. In summary, the synergistic combination of drug carriers and bioactive non-conventional metallodrugs with trackable features is expected to improve the effectiveness of anticancer treatments and decrease, at the same time, their undesirable side effects [27,28].

Taking into account all the above information, here, we have prepared two novel ruthenium metalloarenes based on anthracene units namely, [Ru(*p*-cymene)(L_1)Cl_2] (**1**) and [Ru(*p*-cymene)(L_2)Cl_2] (**2**) (**L_1** = 1-(anthracen-9-yl)-*N*-(pyridin-3-ylmethyl)methanamine; **L_2** = 1-(anthracen-9-yl)-*N*-(pyridin-4-ylmethyl)methanamine). Our studies have revealed that the position of the anthracene moiety clearly affects the fluorescent properties of the resulting Ru(II) complexes, as only **2** shows emission at 442 nm. The interaction of **1** and **2** with different biological targets (DNA, S-donor aminoacid cysteine, cysteine cathepsin B and cathepsin D) has also been evaluated. In addition, we have studied the biological properties of the isolated compounds demonstrating *in vitro* cytotoxicity against HL-60 cancer cell line occurring *via* apoptosis. Finally, we have successfully encapsulated these ruthenium metallodrugs into two well-known biocompatible and stable mesoporous silicas (MCM-41 and SBA-15) using two different incorporation strategies (impregnation and grinding).

2. Experimental Section

2.1. Methods

N_2 adsorption isotherms were measured at 77 K on a Micromeritics Tristar 3000 volumetric instrument. Prior to measurement, samples were activated by heating and outgassing at 10^{-4} bar. Elemental (C, H, N) analyses were obtained at a Flash EA1112 CHNS-O (Centre of Scientific Instrumentation of the University of Jaén). The infrared spectra were recorded using a Perkin Elmer Spectrum GX IR spectrometer. Thermogravimetric analysis were performed using

a Mettler Toledo TGA/DSC STAR system under oxygen flow (20 mL min^{-1}) running from RT to 1173 K with a heating rate of 2 K min^{-1}. ^{1}H-^{1}H COSY NMR experiments for the characterization of $\mathbf{L_1}$ and $\mathbf{L_2}$ (DMSO-d^6), and **1** and **2** ($CDCl_3$) were recorded on a VARIAN DIRECT DRIVE (500 MHz) instrument. ^{1}H-^{1}H NOESY NMR experiments for the characterization of $\mathbf{L_1}$ and $\mathbf{L_2}$ (DMSO-d^6) were recorded on a VARIAN DIRECT DRIVE (400 MHz) instrument. ^{1}H NMR experiments for the characterization of **1**, **2** and [Ru(*p*-cymene)Cl_2]$_2$ and the interaction of **2** with cysteine, were performed in 0.75 mL of $CDCl_3$ solution with 5 mg of **2** and two equivalents of cysteine at 293 K. The ^{1}H NMR experiments were recorded on a VARIAN INOVA UNITY (300 MHz). All the NMR measurements were performed in the Centre of Scientific Instrumentation of the University of Granada. The diffuse reflectance spectra were obtained in a VARIAN, model CARY-5E, while the emission spectrum of **2** and DNA binding assays were recorded in a Cary Eclipse Fluorescence Spectrophotometer (parameters for fluorescence spectra of **2**: λ_{em}: 440 nm, λ_{ex} = 362 nm, $slits_{em}$ = 10.0 nm, $slits_{ex}$ = 10.0 nm; parameters for DNA binding assays: λ_{em} = 600 nm, λ_{ex} = 540 nm, $slits_{em}$ = 15.0 nm, $slits_{ex}$ = 10.0 nm). High Resolution Transmission Electron Microscopy (HR-TEM) and Energy-dispersive X-ray Spectroscopy (EDX) were performed using a STEM PHILIPS CM20 HR microscope equipped with an EDX spectrometer operating at an accelerating voltage of 200 KeV. Samples were prepared by dispersing a small amount of the material (3 mg) in absolute ethanol (1 mL) followed by sonication for 10 minutes and deposition on copper grid (Centre of Scientific Instrumentation of the University of Granada). Flow cytometry studies were performed in a BECTON DICKINSON FACS Vantage equipment and cell images were recorded using a confocal laser scanning microscope (Leica DM5500B) with a 63x oil immersion objective. The 363 nm line from a blue diode laser was used for excitation between 465 and 700 nm, and emission was collected between 412 and 437 nm (DAPI) and 524 and 552 nm (compound **2**). Both equipments are located in the Centre of Scientific Instrumentation of the University of Granada.

2.2. Synthesis of materials

All chemicals were commercially available and used without further purification.

Synthesis of [Ru(p-cymene)Cl_2]$_2$. The method reported by Smith *et al.* [29] was followed. Yield: 83%. ^{1}H NMR (300 MHz, $CDCl_3$) δ: 5.47 (d, 4H), 5.34 (d, 4H), 2.91 (m, 1H), 2.15 (s, 6H), 1.27 (d, 12H). Anal. calc. for ($RuC_{10}H_{14}Cl_2$)$_2$: C, 39.23; H, 4.61 ; Anal. found: C, 38.87; H, 4.44. Calculated residue after thermal treatment of [Ru(*p*-cymene)Cl_2]$_2$: RuO_2: 43.46%; Found: 42.43%.

*Synthesis of 1-(anthracen-9-yl)-N-(pyridin-3-ylmethyl)methanamine (**L_1**).* The reaction of 3-picolylamine (200 µL, 2 mmol) with 9-anthraldehyde (206.24 mg, 1 mmol) in absolute ethanol (80 mL) under reflux during 2 h gave rise to a yellow limpid solution. The mixture was evaporated to near dryness and $\mathbf{L_1}$ was precipitated by water addition and collected as a spectroscopically pure yellow solid in good yield (257.24 mg, 86%). ^{1}H NMR (500 MHz, DMSO-

d_6) δ: 9.74 (s, 1H), 8.73 (m, 2H), 8.65 (d, 2H), 8.52 (m, 1H), 8.14 (d, 2H), 7.91 (d, 1H), 7.57 (m, 4H), 7.43 (m, 1H), 5.14 (s, 2H) (Fig. S1).

*Synthesis of 1-(anthracen-9-yl)-N-(pyridin-4-ylmethyl)methanamine (**L_2**).* The same procedure as for the synthesis of **L_1** was followed, using 4-picolylamine instead of 3-picolylamine. **L_2** was obtained as a spectroscopically pure yellow solid in good yield (250.0 mg, 84%). ^{1}H NMR (500 MHz, DMSO-d_6) δ: 9.73 (s, 1H), 8.72 (s, 1H), 8.67 (d, 2H), 8.58 (d, 2H), 8.15 (d, 2H), 7.57 (m, 4H), 7.49 (d, 2H), 5.13 (s, 2H) (Fig. S2).

*Synthesis of [Ru(p-cymene)(L_1)Cl_2] (**1**).* The reaction of [Ru(*p*-cymene)Cl_2]$_2$ (153 mg, 0.25 mmol) with **L_1** (149.19 mg, 0.5 mmol) in chloroform (30 mL) under nitrogen at reflux during 5 h lead to a red solution. After cooling, the solvent was allowed to evaporate till a red-orange precipitate appeared. Compound **1** was collected in a good yield (76%). ^{1}H NMR (300 MHz, $CDCl_3$) δ: 9.67 (s, 1H), 9.19 (s, 1H), 8.99 (m, 1H), 8.70 (s, 1H), 8.57 (d, 2H), 8.05 (d, 2H), 7.68 (m, 1H), 7.57 (m, 4H), 7.34 (t, 1H), 5.42 (d, 2H), 5.20 (d, 2H), 5.12 (s, 2H), 2.94 (m, 1H), 2.07 (s, 3H), 1.24 (d, 6H) (Fig. S3). Anal. calc. for ($C_{31}RuCl_2H_{30}N_2$)(H_2O)$_{0.5}$ (**1**): C, 60.88; N, 4.58; H, 5.11; Anal. found: C, 60.46; N, 4.43; H, 5.39. Calculated residue after thermal treatment of [Ru(*p*-cymene)(L_1)Cl_2]: RuO_2: 21.44%; Found: 21.03%.

*Synthesis of [Ru(p-cymene)(L_2)Cl_2] (**2**).* The same procedure as for the synthesis of **1** was followed but performing the reaction under nitrogen at room temperature during 6 h. Compound **2** was collected in a good yield (78%). ^{1}H NMR (300 MHz, $CDCl_3$) δ: 9.63 (s, 1H), 9.00 (d, 2H, *J* = 6.00 Hz), 8.53 (m, 3H), 8.04 (d, 2H), 7.53 (m, 4H), 7.45 (d, 2H), 5.42 (d, 2H), 5.20 (d, 2H), 5.14 (s, 2H), 2.98 (s, 3H), 2.09 (s, 3H), 1.29 (d, 6H) (Fig. S4). Anal. calc. for $C_{31}RuCl_2H_{30}N_2$ (**2**): C, 61.79 ; N, 4.65 ; H, 5.02; Anal. found: C, 61.47; N, 4.78; H, 5.27. Calculated residue after thermal treatment of [Ru(*p*-cymene)(L_2)Cl_2]: RuO_2: 21.76%; Found: 21.05%. In ethanol, compound **2** has fluorescence excitation/emission maxima at 362 and 440 nm, respectively.

Synthesis of MCM-41. MCM-41 was prepared according to the sol-gel method previously described [30].

Synthesis of SBA-15. The SBA-15 mesophase was synthesized according to the procedure followed by Zhao *et al*. [31,32].

2.3. Ru(II) metallodrugs incorporation

Evacuation and activation of MCM-41 and SBA-15. Prior to the loading of the ruthenium compounds into the different porous matrixes (MCM-41 and SBA-15), the as synthesized solids were heated under vacuum (423 K, 5 h) in order to achieve the complete removal of the solvent guest molecules and obtain empty pores ready for adsorption of the ruthenium metallodrugs.

Stability studies. The chemical stability of MCM-41 and SBA-15 was studied under two different encapsulation conditions (impregnation in CH_2Cl_2 and grinding in acetone) in order to establish the potential use of these methods for the incorporation of the ruthenium complexes **1** and **2** into the matrixes. In a typical test, 100 mg of activated material were suspended in 100 mL of CH_2Cl_2 for 24 h at room temperature or were grinded in 20 mL of acetone until all the solvent was gone (*ca.* 20 min). Afterwards, the solids were filtered off and dried at 393 K under vacuum (10^{-4} bar) for 7 h before the isotherm acquisition (N_2, 77 K, Figure S11).

Drug encapsulation by impregnation method. The solid-liquid adsorption experiments were performed at room temperature by suspending 100 mg of activated matrix in 10 mL of a 16 mM CH_2Cl_2 solution of **1** or **2**. After 24 h of stirring, to assure that the equilibrium was reached, each sample was filtered off and washed with CH_2Cl_2 (10 mL x 3). The amount of incorporated metallodrug was calculated by elemental and thermogravimetric analysis (see supporting information).

Drug encapsulation by mechanochemical method. In a typical experiment, 100 mg (0.16 mmol) of **1** or **2** were dissolved in 20 mL of acetone. Then, 100 mg of activated matrix were added and the mixture was grinded in order to speed up the solvent evaporation and progressively concentrate the solution of the corresponding metallodrug. This procedure was carried out until all the solvent was evaporated. Finally, the solid product was washed with acetone (10 mL x 5) in order to eliminate the excess of non-adsorbed drug. The amount of incorporated metallodrug was calculated by elemental and thermogravimetric analysis (see supporting information).

2.4. Biological studies

Cell culture and viability assays. Leukemia cells HL-60, obtained from the Centre of Scientific Instrumentation of the University of Granada (ECACC No. 98070106), were cultivated as a suspension in RPMI-1640 medium (Sigma Aldrich R5886) supplemented with 20% FBS (Sigma Aldrich F4135), 4 mM L-glutamine (Sigma Aldrich G7513), 1 mM sodium pyruvate (Sigma Aldrich S8636) and 4.5 mg mL^{-1} glucose. Cells were incubated at 37 °C in a humidified atmosphere with 5% CO_2 and maintained using standard cell cultures techniques. Cytotoxicity of the ligands ($\mathbf{L_1}$ and $\mathbf{L_2}$) and the corresponding ruthenium complexes (**1** and **2**) was determined by flow cytometry. Briefly, cells were suspended at a final concentration of 3×10^5 cells/mL in a 24-well plate (500 µL/well) in the presence of different suspensions of each drug in the cellular medium (500-1 µM) due to the poor solubility of these drugs in water. After 48 h of treatment, 100 µL per well of propidium iodide solution (100 mg/mL) was added and incubated for 10 min at 37 °C in darkness. Afterwards, 100 µL per well of fluorescein diacetate (100 ng/mL) was added and incubated under the same conditions (37 °C, 10 min). Finally, the cells were recovered by centrifugation (400 *g*, 10 min) and the pellet was re-dissolved in PBS and

analysed by flow cytometry. The percentage viability was calculated in comparison with a control culture.

Apoptosis tests. HL-60 cells were suspended at a density of 0.5 x 10^6 cells/mL in a 24-well plate (500 µL/well) in the presence of IC_{25} concentration of each drug. After 24 h of treatment, cells were analysed by flow cytometry using an Annexin V-FTIC apoptosis detection kit from Inmmunostep. Briefly, cells were washed twice with temperate PBS and resuspended in 100uL of Annexin binding buffer. Then, 5 µL of the Annexin V-FTIC and 5 µL of propidium iodide were added and the cells were incubated in the dark (15 min, 37 °C) previous to the analysis. Non-treated cells were used as control. Data were analysed using the FACSDiva software.

Uptake assays by confocal microscopy. Confocal laser scanning microscopy was used to study the accumulation of the native ruthenium compound **2** in monolayer cultures of living HL-60. For this purpose, HL-60 cells were plated (10^5 cells/dish) and left to grow for 24 h. Then, compound **2** was added to the wells (final concentration 25 µM) and cells were further incubated for 30 minutes. Afterwards, cells were rinsed twice with PBS to remove residual extracellular drug, fixed in formaldehyde (0.25 %) in darkness for 15 min and washed again with PBS. Finally, cells were incubated for 5 min with DAPI (4',6-diamidino-2-phenylindole, 300 nM) and rinsed twice with PBS to remove free DAPI. Images were recorded using a confocal laser scanning microscope (Leica DM5500B).

Uptake assays by flow cytometry. Flow cytometry was also used to analyse the mechanism of uptake of compound **2**. HL-60 cells were plated (10^5 cells/dish) and left to grow for 24 h. Then, compound **2** was added (final concentration 25 µM) and cells were further incubated for 30 minutes at 37 or 4 °C in darkness. Afterwards, the cells were recovered by centrifugation (400 g, 10 min) and the pellet was re-dissolved in PBS and analysed by flow cytometry. Non-treated cells were used as control. Data were analysed using the FACSDiva software.

Ethidium bromide displacement assays. DNA interaction of both ligands ($\mathbf{L_1}$ and $\mathbf{L_2}$) and ruthenium complexes (**1** and **2**) was studied by measuring the quenching of ethidium bromide (EB) fluorescence as it leaves the protection of ct-DNA (calf thymus DNA). A ct-DNA/salts/buffer solution with EB (ct-DNA:EB; 4 µM : 5 µM) was prepared. The emission spectra were recorded as a function of ligand or complex concentration. The investigated compound concentration was slowly increased for ct-DNA (pair base)/compound ratios from 200:1 to 1:1 keeping the ct-DNA and EB concentrations constant.

Cathepsin B enzymatic assay. Crude Bovine Spleen Cathepsin B (C6286) was purchased from Sigma-Aldrich and used without further purification. The colorimetric assay was performed in 20 mM sodium acetate and 1 mM EDTA (adjust to pH 5.1 with HCl 1 M), using Na-CBZ-L-lysine *p*-nitrophenyl ester (CBZ = *N*-carbobenzoxy) as substrate. For the enzyme to be

catalytically functional, the active site cysteine needs to be in the reduced form. Therefore, prior use, cathepsin B was pre-reduced with dithiothretiol (DTT) to ensure that the majority of the enzyme is in a catalytically active form. Thus, cathepsin B was activated, before dilution, in the presence of an excess of DTT (1.2 eq) for 1 h at 303 K. IC_{50} determinations were performed in triplicate using a fixed enzyme concentration of 200 nM and a fixed substrate concentration of 100 µM. The enzyme and inhibitor were co-incubated at 303 K over a period of 24 h prior to the addition of substrate. Activity was measured over 500 min at 326 nm. Concentration of inhibitor was ranged between 0.3 and 100 µM. The cathepsin B enzymatic assays were performed using **L_1**, **L_2**, **1** and **2** as inhibitors.

Cathepsin D enzymatic assay. Cathepsin D Fluorimetric assay kit (CS0800) and Crude Bovine Spleen Cathepsin D (C3138) were purchased from Sigma-Aldrich and used without further purification. The fluorimetric assay was performed in a Sigma-Aldrich Assay Buffer (A3855) with 2.5% Albumin Solution (A3980), using MCA-Gly-Lys-Pro-Ile-Leu-Phe-Phe-Arg-Leu-Lys(DNP)-D-Arg-NH_2 trifluoroacetate salt as substrate (1 mM solution, C4492). The final concentrations used in this assay were ca. 5 nM (cathepsin D), 20 µM (substrate), and 50-200 µM (**2**) or 500 µM (**L_1**, **L_2** and **1**, respectively). The inhibition of the cathepsin D enzymatic activity by **2** is confirmed by the horizontal slope of the curve representing the hydrolysis of the substrate *vs* time at 200 µM. On the contrary, in the presence of both ligands and complex **1**, the progressive hydrolysis of the substrate takes place, demonstrated by an increase of the fluorescence intensity *vs* time, confirming the non inhibition of the enzymatic activity of cathepsin D by these compounds even at 500 µM (Figure S9).

3. Results and discussion

3.1. Design, synthesis and characterization of the two novel Ru(II)-metallodrugs

The synthesis of two novel metallodrugs [Ru(η^6-*p*-cymene)(L_1)Cl_2] (**1**) and [Ru(η^6-*p*-cymene)(L_2)Cl_2] (**2**) was readily achieved, in a two-step synthesis, as outlined in Scheme 1. The corresponding ligands, 1-(anthracen-9-yl)-*N*-(pyridin-3-ylmethyl)methanamine (**L_1**) and 1-(anthracen-9-yl)-*N*-(pyridin-4-ylmethyl)methanamine (**L_2**), both containing an anthracene unit, were designed to confer potential trackable properties to the resulting metallodrugs. Specifically, these ligands were obtained by reacting 9-anthraldehyde with 3-picolylamine (in **L_1** synthesis) or 4-picolylamine (in **L_2** synthesis) in absolute ethanol under reflux. The success of this reaction was confirmed by NMR spectroscopy as the characteristics signals of both organic moieties, slightly shifted, were present.

In addition, a significant displacement of the methyne (from 3.74 to 5.14 ppm) and methylene (from 11.44 to 9.74 ppm) protons next to the imine group was observed, which clearly confirmed the formation of the coupling (Fig. S1). The exact attribution of all the proton signals in **L_1** and **L_2** was achieved by ^{1}H-^{1}H COSY and NOESY experiments (Fig. S2 and S3). The subsequent reaction of the anthracene derivatives **L_1** and **L_2** with the dimeric precursor [η^6-*p*-cymene)$RuCl_2]_2$ gave the corresponding Ru(II) metallodrugs **1** and **2**. The composition of these complexes was established by elemental and thermogravimetric analyses (see experimental section). Besides, ^{1}H NMR spectroscopy confirms the presence of the characteristic signals of **L_1** or **L_2** and the cymene unit. The complete assignment of the signals can be found in the supporting information (Fig. S4 and S5). Noteworthy, **1** and **2** are very soluble in low polar solvents (CH_2Cl_2, $CHCl_3$, acetone) while in polar solvents (H_2O, MeOH, EtOH) are poorly soluble. This fact might be attributed to the presence of apolar residues (anthracene and cymene moieties) in these systems. The low water solubility of these systems confirms the necessity of using delivery vehicles in order to exploit their potential biological properties in full.

In order to confirm the potential use of these Ru(II) complexes as trackable drugs, we studied their fluorescent properties. As expected, **L_1** and **L_2** showed fluorescence in the blue region due to the presence of the anthracene moiety (Fig. S6). Regarding the metal complexes, **2** exhibited an emission band centred at 442 nm while **1** did not show any fluorescence. This result clearly reveals the influence of the [Ru(*p*-cymene)Cl_2] linking position, where the ortho-substituted picolylamine design in compound **2** seems to contribute to extend the π delocalization.

3.2. Activity against different biological targets

Taking into account the extended aromatic nature of **L_1** and **L_2**, we firstly studied the DNA-intercalating features of the free ligands as well as of complexes **1** and **2**, by means of competitive binding with ethidium bromide (EB). According to our results, no changes in the fluorescence spectra of EB are observed upon addition of increasing quantities of the compounds under study suggesting that these anthracene-based derivatives may show weaker intercalating properties than EB (Fig. S7).

Then, we investigated the biological activity of **1** and **2** towards other biorelevant targets (amino acids and proteases). In fact, we observed that our Ru complexes react with the amino acid cysteine, as previously found in related half-sandwich Ru(II) systems, in which this S-donor ligand is coordinated [28,33,34]. The ^{1}H NMR spectroscopy studies revealed that incubation of **1** or **2** ($CDCl_3$, 37 °C) with pure cysteine led to a rather fast (< 4h) interaction between the corresponding complex and the amino acid provoking the breakdown of **L_1** and **L_2** with the

concomitant liberation of the free anthracene moiety. The resulting cysteine Ru(II) complex precipitates in the medium and, as a consequence, cymene and picolylamine proton signals are missing in the NMR spectra (Fig. S8). Similar results were previously observed by our group [35].

On the other hand, **1** and **2** inhibited the protease activity of cysteine cathepsin B (Fig. 1), exhibiting an IC_{50} value of 9.9 and 8.0 μM, respectively. These values are in the same order of magnitude that the ones previously reported for RAPTA-C (IC_{50} = 2.5 μM)[12] and other Ru-based metallodrugs [36], as well as the corresponding free ligands, $\mathbf{L_1}$ and $\mathbf{L_2}$ (Fig. S9). Regarding the interaction with aspartic cathepsin D, fluorescence binding assays demonstrated a moderate IC_{50} value of approximately 168 μM for compound **2** and a non-relevant inhibition of the enzymatic activity of this protease after its incubation with a 500 μM solution of complex **1** (Fig. 1 and S9). It should be noted that free $\mathbf{L_1}$ and $\mathbf{L_2}$ ligands did not affect substrate hydrolysis rate, which points that, in this case, protease inhibition activity might be related to Ru binding ability to amino acids (see above). These results may be of interest in view of the exacerbated metabolism of these types of enzymes in cancer cells [9,34].

3.3. Viability studies and cellular uptake

Taking into account the interaction of **1** and **2** with biorelevant targets, such as cysteine and cathepsin B, we evaluated the *in vitro* cytotoxicity of both anthracene ligands ($\mathbf{L_1}$ and $\mathbf{L_2}$) and ruthenium complexes (**1** and **2**) towards leukemia cell line HL-60 by flow cytometry. The results revealed that **1** and **2** are slightly more toxic than the corresponding ligands (IC_{50} values: 103.1, 97.7, 84.5 and 87.0 μM for $\mathbf{L_1}$, $\mathbf{L_2}$, **1** and **2**, respectively), and in the same order of magnitude than the reference compound KP1019, indazolium *trans*-[tetrachlorobis(1H-indazole)ruthenate(III)], (IC_{50} value: 56.0 μM) [37]. Further flow cytometry studies confirmed that the observed toxic effects of these molecules occur *via* apoptosis. Indeed, in the presence of IC_{25} concentration of each drug non necrotic cells were observed after 24 h of treatment (Fig. S10).

On the other hand, taking advantage of the fluorescence properties of compound **2** (Fig. S6), confocal laser scanning microscopy was used to confirm the accumulation *in vitro* of this metallodrug into leukemia cells HL-60. Indeed, compound **2** accumulated rapidly into the cytoplasm of this cell line (Fig. 2). In order to better understand the mechanism of uptake of this ruthenium drug, cells were incubated for 30 min with complex **2** (final concentration: 25 μM) at 4 and 37 °C. Afterwards, the cells were analysed by flow cytometry by means of the characteristic fluorescence of the ruthenium complex. The results demonstrated again a rapid accumulation of **2** inside the cells at 37 °C, as indicated by a significant increase (*ca.* 22.3%) in fluorescence intensity on treated

cells compared to non-treated ones. A similar result was observed at 4 °C (fluorescence intensity increase *ca.* 18.6%), which clearly confirms that the uptake of this ruthenium metallodrug occurs mainly by passive diffusion, as it has been previously reported for other lipophilic drugs [38].

3.4. Encapsulation of the Ru(II)-metallodrugs in different porous matrixes

Taking into account the potential protease inhibition activity and low water solubility of **1** and **2**, we decided to study the incorporation of these ruthenium metallodrugs into two well-known mesoporous silicas, namely, MCM-41 and SBA-15, as a proof of concept investigation of metallodrug vehiculization.

All mesoporous materials were prepared and characterized as detailed in the Experimental Section. After the isolation of these porous matrixes, a thermal activation process was carried out in order to remove the structure directing molecules encapsulated into the pores. This post-synthetic treatment leaves large empty cavities (20-100 and 46-300 Å in MCM-41 and SBA-15, respectively) of apropriate size for adsorption of the ruthenium metallodrugs (*ca.* 1.5 nm) designed in this work. In order to better optimize the incorporation of **1** and **2** into the porous matrixes, two encapsulation strategies (impregnation and solvent assisted grinding method) were employed (Fig. 3).

It should be noted that the chemical stability of the activated matrixes, under the encapsulation experimental conditions, was previously tested in order to check the suitability of the drug incorporation methodology. According to our results, similar N_2 adsorption profiles were observed after both treatments, while the BET surface values slightly decrease (20-30%) when comparing the treated materials with the pristine ones (Fig. S11). In view of these results, the suitability of both experimental conditions for the encapsulation of **1** and **2** metallodrugs into the pores of MCM-41 and SBA-15 was confirmed.

Afterwards, we studied the loading of **1** and **2** into the porous matrixes by using the strategies mentioned above: *i)* impregnation of the activated matrixes in saturated dichloromethane solutions of the corresponding ruthenium complexes; and *ii)* grinding of the activated matrixes in saturated acetone solutions of the corresponding metallodrugs. Thus, eight hybrid materials were initially prepared and characterized by elemental and thermogravimetric analysis (see supporting information). While the highest loading for each drug was achieved in MCM-41 by the grinding strategy (0.02 and 0.08 mmol of drug per mmol of matrix or 0.17 and 0.46 g of drug per g of dried material, for **1** and **2**, respectively), similar loadings were accomplished in SBA-15 (*ca.* 0.03 mmol of drug per mmol of matrix, or *ca.* 0.23 g of drug per g of dried material). From now onwards, the

remaining studies have been performed only on the hybrid materials with the highest cargo for each metallodrug (Table S1).

The actual incorporation of the designed Ru(II) complexes into the porous materials was proven by: *i)* the dramatic reduction of the adsorption capacity of the mesoporous matrixes (BET drops from 591 m^2 g^{-1} (SBA-15_impregnation) to 215 m^2 g^{-1} (**SBA-15@1**) and to 191 m^2 g^{-1} (**SBA-15@2**); and from 1030 m^2 g^{-1} (MCM-41_grinding) to 335 m^2 g^{-1} (**MCM-41@1**) and to 16 m^2 g^{-1} (**MCM-41@2**) (Fig. 4, Table S2); *ii)* the presence of the main characteristic peaks of pure **1** or **2** compounds in the IR spectra of the loaded matrixes (Fig. S12); *iii)* a weight loss on the thermogravimetric analysis of the hybrid systems related to the drug decomposition (Fig. S13); *iv)* the appearance, in the diffuse reflectance spectra of the loaded matrixes, of a characteristic absorption band in the visible region for these Ru complexes (Fig. S14) and *v)* energy-dispersive X-ray spectroscopy (EDX) analysis (Fig. S15).

Finally, high resolution transmission electron microscopy (HR-TEM) of the loaded materials revealed that **MCM-41@1** and **MCM-41@2** were isolated as nanoparticles with an average size of *ca.* 40 nm with EDX analysis showing the presence of Si and Ru (Fig. S15 and S16).

4. Conclusions

In this work, we have prepared two novel anthracene-based Ru(II) complexes, one of them showing fluorescence properties. This feature has been exploited to visualize the uptake of this metallodrug into leukemia cells HL-60, as well as to demonstrate that the main cellular uptake mechanism takes place by passive diffusion. Moreover, both ruthenium complexes have shown *in vitro* cytotoxic activity towards this cancer cell line taking place *via* apoptosis. Further studies have demonstrated that these ruthenium complexes seem to show weaker intercalating features towards DNA than ethidium bromide. However, they inhibit the enzymatic activity of cysteine cathepsin B, which is overexpressed in some cancer cells, as well as interact with S-donor aminoacid cysteine. These results point out that the cytotoxic mechanism of these compounds might be associated to their interaction with cysteine containing biomolecules rather than DNA. Finally, two different encapsulation strategies have been optimized in order to successfully incorporate these Ru drugs into the pores of two well-known mesoporous silicas. In this regard, as a proof of concept, the present work shows the possibility of using these biocompatible mesoporous matrixes as vehicles of theranostic metallodrugs.

FIGURES

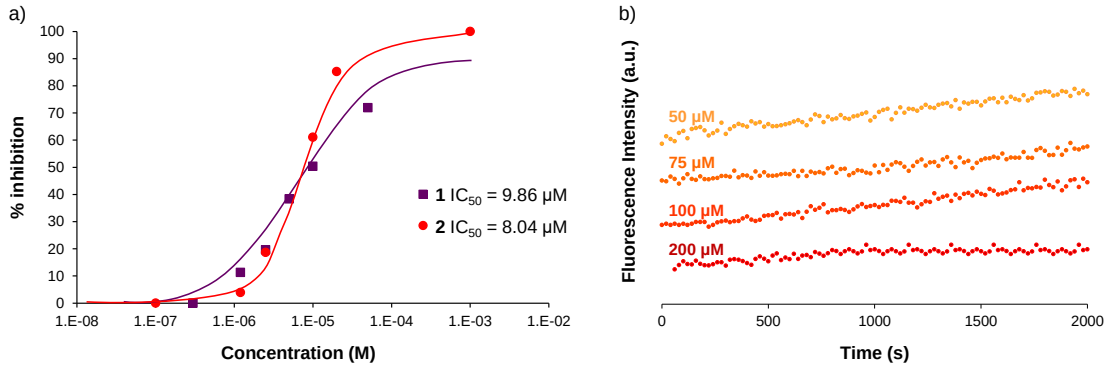

Fig. 1. (a) IC_{50} curves for the inhibition of cathepsin B by **1** and **2**. (b) Cathepsin D enzymatic fluorescence assays confirming the inhibition of its enzymatic activity by **2** at 200 µM.

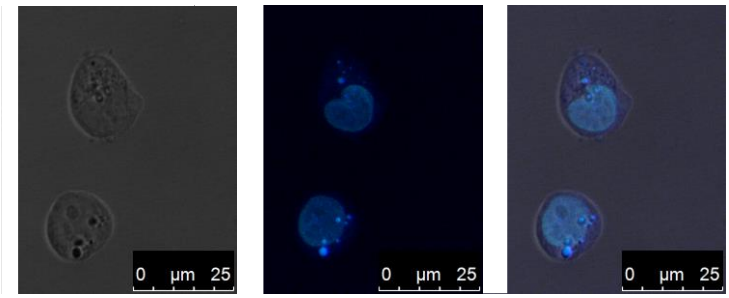

Fig. 2. Bright field, fluorescence and overlay images showing cellular accumulation and distribution of compound **2** (turquoise) and DAPI (blue, cell nucleus) in HL-60 cells after 30 min of incubation.

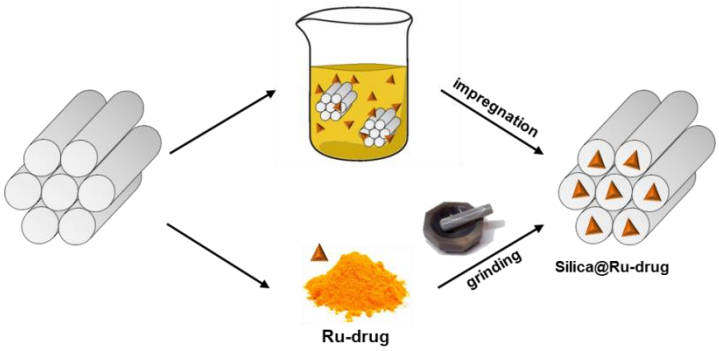

Fig. 3. Encapsulation strategies followed for the incorporation of these Ru(II) metallodrugs into the selected silica porous matrixes.

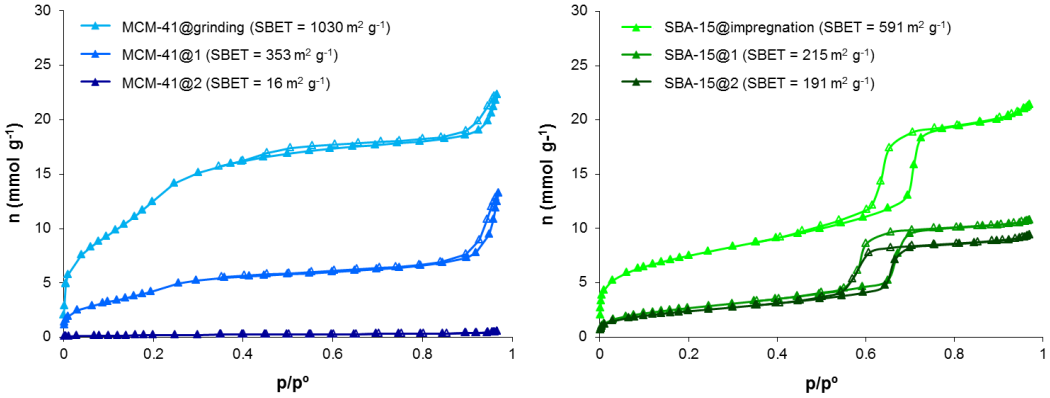

Fig. 4. N_2 (77 K) adsorption isotherms of the empty and loaded porous materials. Empty symbols denote desorption.

SCHEMES

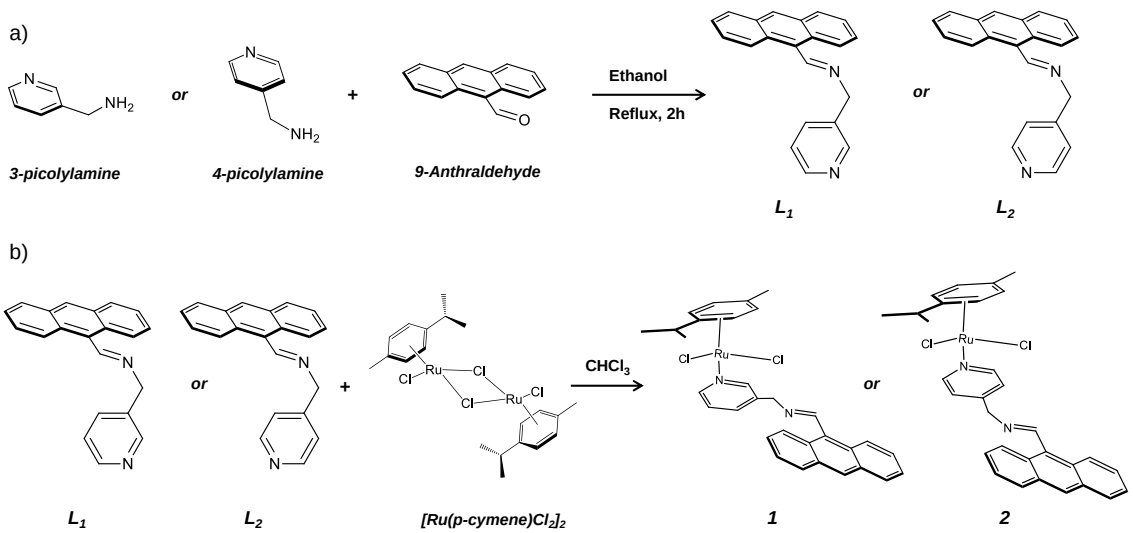

Scheme 1. (a) Reaction of 3-picolylamine or 4-picolylamine with 9-anthraldehyde to give the fluorescent ligand 1-(anthracen-9-yl)-*N*-(pyridin-3-ylmethyl)methanamine (**L_1**) or 1-(anthracen-9-yl)-*N*-(pyridin-4-ylmethyl)methanamine (**L_2**). (b) Synthesis of [Ru(*p*-cymene)(L_1)Cl_2]$_2$ (**1**) or [Ru(*p*-cymene)(L_2)Cl_2]$_2$ (**2**) starting from **L_1** or **L_2** and the dimer [Ru(*p*-cymene)Cl_2]$_2$.

Acknowledgements

The Spanish Ministry of Economy and Competitivity and UE Feder Program (projects CTQ2014-53486R and CRM Juan de la Cierva Contract), Junta de Andalucía (project P09-FQM-4981 and SR postdoctoral contract), CEI BioTic Granada (project CEI2015-MP-BS39) and COST action CM1105 are gratefully acknowledged for generous funding.

References

[1] M.A. Jakupec, M. Galanski, V.B. Arion, C.G. Hartinger, B.K. Keppler, Antitumour metal compounds: more than theme and variations, Dalt. Trans. (2008) 183–194. doi:10.1039/b712656p.

[2] B.C.S. Allardyce, P.J. Dyson, Ruthenium in Medicine: Current Clinical Uses and Future Prospects, Platin. Met. Rev. 45 (2001) 62–69.

[3] W. Han Ang, P.J. Dyson, Classical and Non-Classical Ruthenium-Based Anticancer Drugs: Towards Targeted Chemotherapy, Eur. J. Inorg. Chem. (2006) 4003–4018. doi:10.1002/ejic.200600723.

[4] C.A. Vock, W.H. Ang, C. Scolaro, A.D. Phillips, L. Lagopoulos, L. Juillerat-Jeanneret, et al., Development of ruthenium antitumor drugs that overcome multidrug resistance mechanisms, J. Med. Chem. 50 (2007) 2166–2175. doi:10.1021/jm070039f.

[5] L. Brescacin, A. Masi, G. Sava, A. Bergamo, Effects of the ruthenium-based drug NAMI-A on the roles played by TGF-β1 in the metastatic process, J. Biol. Inorg. Chem. 20 (2015) 1163–1173. doi:10.1007/s00775-015-1297-8.

[6] W. Cao, W. Zheng, T. Chen, Ruthenium Polypyridyl Complex Inhibits Growth and Metastasis of Breast Cancer Cells by Suppressing FAK signaling with Enhancement of TRAIL-induced Apoptosis, Sci. Rep. 5 (2015) 9157–9168. doi:10.1038/srep09157.

[7] W.H. Ang, A. Casini, G. Sava, P.J. Dyson, Organometallic ruthenium-based antitumor compounds with novel modes of action, J. Organomet. Chem. 696 (2011) 989–998. doi:10.1016/j.jorganchem.2010.11.009.

[8] V. Brabec, O. Nováková, DNA binding mode of ruthenium complexes and relationship to tumor cell toxicity, Drug Resist. Updat. 9 (2006) 111–122. doi:10.1016/j.drup.2006.05.002.

[9] A. Casini, F. Edafe, M. Erlandsson, L. Gonsalvi, A. Ciancetta, N. Re, et al., Rationalization of the inhibition activity of structurally related organometallic compounds against the drug target cathepsin B by DFT, Dalt. Trans. 39 (2010) 5556–5563. doi:10.1039/c003218b.

[10] B. Wu, M.S. Ong, M. Groessl, Z. Adhireksan, C.G. Hartinger, P.J. Dyson, et al., A ruthenium antimetastasis agent forms specific histone protein adducts in the nucleosome core, Chem. Eur. J. 17 (2011) 3562–3566. doi:10.1002/chem.201100298.

[11] M. Babak, S.M. Meier, K. Huber, J. Reynisson, A. Legin, M. Jakupec, et al., Target Profiling of an Antimetastatic RAPTA Agent by Chemical Proteomics: Relevance to the Mode of Action, Chem. Sci. (2015) 2449–2456. doi:10.1039/C4SC03905J.

[12] A. Casini, C. Gabbiani, F. Sorrentino, M.P. Rigobello, A. Bindoli, T.J. Geldbach, et al., Emerging protein targets for anticancer metallodrugs: inhibition of thioredoxin reductase and cathepsin B by antitumor ruthenium(II)-arene compounds, J. Med. Chem. 51 (2008) 6773–6781. doi:10.1021/jm8006678.

[13] P. Zhang, H. Huang, Y. Chen, J. Wang, L. Jin, H. Chao, Ruthenium(II) anthraquinone complexes as two-photon luminescent probes for cycling hypoxia imaging in vivo, Biomaterials. 53 (2015) 522–531.

[14] A. Son, A. Kawasaki, D. Hara, T. Ito, K. Tanabe, Phosphorescent ruthenium complexes with a nitroimidazole unit that image oxygen fluctuation in tumor tissue, Chem. Eur. J. 21 (2015) 2527–2536. doi:10.1002/chem.201404979.

[15] Y. Niu, F. Han, Q. Zhang, T. Xie, L. Lu, S. Li, et al., Off/On fluorescent chemosensors for organotin halides based on binuclear ruthenium complexes, Angew. Chem. Int. Ed. 52 (2013) 5599–5603. doi:10.1002/anie.201209549.

[16] G. Valenti, E. Rampazzo, E. Biavardi, E. Villani, G. Fracasso, M. Marcaccio, et al., An electrochemiluminescence-supramolecular approac to sarcaosine detection for early diagnosis of prostate cancer, Faraday Discuss. 185 (2015) 299–309.

[17] M.R. Gill, J.A. Thomas, Ruthenium(II) polypyridyl complexes and DNA—from structural probes to cellular imaging and therapeutics, Chem Soc Rev. 41 (2012) 3179–3192. doi:10.1039/c2cs15299a.

[18] P. Liu, B.-Y. Wu, J. Liu, Y.-C. Dai, Y.-J. Wang, K.-Z. Wang, DNA Binding and Photocleavage Properties, Cellular Uptake and Localization, and in-Vitro Cytotoxicity of Dinuclear Ruthenium(II) Complexes with Varying Lengths in Bridging Alkyl Linkers, Inorg. Chem. 55 (2016) 1412–1422.

[19] O. Mazuryk, M. Maciuszek, G. Stochel, F. Suzenet, M. Brindell, 2-Nitroimidazole-ruthenium polypyridyl complex as a new conjugate for cancer treatment and visualization, J. Inorg. Biochem. 134 (2014) 83–91. doi:10.1016/j.jinorgbio.2014.02.001.

[20] Q. Liu, W. Xia, Mesoporous Silica Nanoparticles for Cancer Therapy, in: New Adv. Dis. Biomarkers Mol. Targets Biomed., 2013: pp. 231–242. doi:10.1007/978-1-62703-456-2.

[21] M. Colilla, B. González, M. Vallet-Regí, Mesoporous silica nanoparticles for the design of smart delivery nanodevices, Biomater. Sci. 1 (2013) 114–134. doi:10.1039/c2bm00085g.

[22] C. Giménez, C. de la Torre, M. Gorbe, E. Aznar, F. Sancenón, J.R. Murguía, et al., Gated mesoporous silica nanoparticles for the controlled delivery of drugs in cancer cells, Langmuir. 31 (2015) 3753–3762. doi:10.1021/acs.langmuir.5b00139.

[23] F. Muhammad, M. Guo, W. Qi, F. Sun, A. Wang, Y. Guo, et al., pH-Triggered Controlled Drug Release from Mesoporous Silica Nanoparticles via Intracellular Dissolution of ZnO Nanolids, J. Am. Chem. Soc. 133 (2011) 8778–8781.

[24] M. Frasconi, Z. Liu, J. Lei, Y. Wu, E. Strekalova, D. Malin, et al., Photo-Expulsion of Surface-Grafted Ruthenium Complexes from Mesoporous Silica Nanoparticles, J. Am. Chem. Soc. 135 (2013) 11603–11613. doi:10.1021/ja405058y.

[25] N.Ž. Knežević, B.G. Trewyn, V.S.-Y. Lin, Functionalized mesoporous silica nanoparticle-based visible light responsive controlled release delivery system, Chem. Comm. 47 (2011) 2817–2819. doi:10.1039/c0cc04424e.

[26] L. He, Y. Huang, H. Zhu, G. Pang, W. Zheng, Y.S. Wong, et al., Cancer-targeted monodisperse mesoporous silica nanoparticles as carrier of ruthenium polypyridyl complexes to enhance theranostic effects, Adv. Funct. Mater. 24 (2014) 2754–2763. doi:10.1002/adfm.201303533.

[27] A.B. Seabra, N. Durán, Nitric oxide-releasing vehicles for biomedical applications, J. Mater. Chem. 20 (2010) 1624–1637. doi:10.1039/b912493b.

[28] N. Han, Q. Zhao, L. Wan, Y. Wang, Y. Gao, P. Wang, et al., Hybrid lipid-capped mesoporous silica for stimuli-responsive drug release and overcoming multidrug resistance, ACS Appl. Mater. Interfaces. 7 (2015) 3342–3351. doi:10.1021/am5082793.

[29] M.A. Bennett, A.K. Smith, Arene ruthenium(II) complexes formed by dehydrogenation of cyclohexadienes with ruthenium(III) trichloride, J. Chem. Soc. Dalt. Trans. (1974) 233–241. doi:10.1039/dt9740000233.

[30] W. Zeng, X.F. Qian, Y.B. Zhang, J. Yin, Z.K. Zhu, Organic modified mesoporous MCM-41 through solvothermal process as drug delivery system, Mater. Res. Bull. 40 (2005) 766–772. doi:10.1016/j.materresbull.2005.02.011.

[31] D. Zhao, Q. Huo, J. Feng, B.F. Chmelka, G.D. Stucky, Tri-, Tetra-, and Octablock Copolymer and Nonionic Surfactant Syntheses of Highly Ordered, Hydrothermally Stable, Mesoporous Silica Structures, J. Am. Chem. Soc. 120 (1998) 6024–6036.

[32] D. Zhao, J. Feng, Q. Huo, N. Melosh, G. Fredrickson, B. Chmelka, et al., Triblock

copolymer syntheses of mesoporous silica with periodic 50 to 300 angstrom pores, Science (80-.). 279 (1998) 548–552. doi:10.1126/science.279.5350.548.

[33] L.E.H. Paul, B. Therrien, J. Furrer, Investigation of the reactivity between a ruthenium hexacationic prism and biological ligands, Inorg. Chem. 51 (2012) 1057–1067. doi:10.1021/ic2021935.

[34] A. Casini, C.G. Hartinger, A.A. Nazarov, P.J. Dyson, Organometallic Antitumour Agents with Alternative Modes of Action, Top. Organomet. Chem. 32 (2010) 57–80. doi:10.1007/978-3-642-13185-1.

[35] S. Rojas, P.S. Wheatley, E. Quartapelle-Procopio, B. Gil, B. Marszalek, R.E. Morris, et al., Metal–organic frameworks as potential multi-carriers of drugs, CrystEngComm. 15 (2013) 9364–9367. doi:10.1039/c3ce41289j.

[36] J. Kljun, I. Bratsos, E. Alessio, G. Psomas, U. Repnik, M. Butinar, et al., New uses for old drugs: attempts to convert quinolone antibacterials into potential anticancer agents containing ruthenium, Inorg. Chem. 52 (2013) 9039–9052. doi:10.1021/ic401220x.

[37] P. Heffeter, M. Pongratz, E. Steiner, P. Chiba, M.A. Jakupec, L. Elbling, et al., Intrinsic and Acquired Forms of Resistance against the Anticancer Ruthenium Compound KP1019 [Indazolium trans - [tetrachlorobis (1 H -indazole) ruthenate (III)] (FFC14A), J. Pharmacol. Exp. Ther. 312 (2005) 281–289. doi:10.1124/jpet.104.073395.chemotherapeutical.

[38] I.D. Goldman, Membrane transport of chemotherapeutics and drug resistance: Beyond the ABC family of exporters to the role of carrier-mediated processes, Clin. Cancer Res. 8 (2002) 4–6.